Manufacture of Pd/Carbon Vulcan XC-72R Nanoflakes Catalysts for Ethanol Oxidation Reaction in Alkaline Media by RoDSE Methodology

Carlos A. Vélez, Juan Corchado, Arnulfo Rojas-Pérez, Edwin J. Serrano-Alejandro, Christian Santos-Homs, Joesene J. Soto-Pérez, and Carlos R. Cabrera*

NSF-CREST Center for Innovation, Research and Education in Environmental Nanotechnology ($CIRE^2N$)
Department of Chemistry, P.O. Box 23346,
University of Puerto Rico, Río Piedras Campus
San Juan, Puerto Rico 00931-3346

Abstract

The Rotating Disk Slurry Electrodeposition (RoDSE) technique is a novel method which can electrochemically deposit metal nanoparticles on a given conductive support and produce a powder catalyst for diverse applications, e.g. ethanol oxidation reaction (EOR). This technique was used to electrodeposit Pd nanoparticles on carbon Vulcan XC–72R nanoflakes at three different applied potentials (0.0, 0.4, and 0.7 V vs. RHE). The potentials were chosen to represent different thermodynamic and kinetic regions of Pd electrodeposition. Each Pd /Vulcan catalyst was characterized through different spectroscopic, microscopic, and electrochemical techniques. Powder X–ray diffraction and transmission electron microscopy studies verified the Pd crystallinity and particle size, respectively. The Pd particle size decreased with a more positive applied electrodeposition potential at carbon Vulcan XC–72R nanoflakes. X-ray photoelectron spectroscopy determined that the applied potential affected, both, the final palladium and carbon oxidation states. Finally, cyclic voltammetry was used to characterize the electrocatalytic activity of each Pd / Vulcan catalyst in 0.1M KOH and for the EOR. It was found that, for Pd electrodeposition using RoDSE, an applied potential of 0.4 V vs. RHE provided considerable harmony between a mass transport and kinetically controlled deposition thereby providing the optimal conditions to produce a better catalyst with better EOR.

Keywords: Pd, RoDSE, Electrodeposition, Ethanol Oxidation Reaction, Vulcan XC-72R

*Corresponding Author: carlos.cabrera2@upr.edu

Introduction

One of the oldest energy conversion devices are fuel cells.[1] They are electrochemical devices that convert chemical energy of a given fuel into electrical energy. Alkaline fuel cells (AFCs), which use hydrogen as fuel and KOH as supporting electrolyte, hold several advantages over other type of fuel cells such as easy handling and relatively low operating temperatures (around 20 – 70 °C). Additionally, the kinetics of the oxygen reduction reaction (ORR) are faster in alkaline media than in acidic conditions, allowing the usage of other non – precious metal catalysts, making the fuel cell economically viable.[1, 2]

However, the main challenge for the commercialization of alkaline fuel cells is the availability of economically viable hydrogen storage technology and the lack of hydrogen transportation and distribution infrastructures. Liquid fuels, such as ethanol and methanol, provide an attractive alternative as fuels in AFCs, because of their easy storage and high energy densities.[3] Although a simpler alcohol, the main disadvantage of using methanol as fuel is that its toxicity is very high, and excessive inhalation can cause blindness or have an effect on the optical nerve.[4-6] On the other hand, ethanol is a bio – fuel, which is less toxic than methanol and can be easily obtained from a variety of feedstock such as corn, sugarcane, wheat or even cellulose. Additionally, much like the ORR, electrochemical oxidation of ethanol is more facile in alkaline media and infrastructures for storage and transportation for ethanol already exist.[4]

A variety of techniques have been employed for the deposition of metal nanoparticles onto different support materials (e.g. chemical and thermal deposition, laser deposition, microwave – assisted, sol – gel among others).[7-9] Moreover, electrodeposition techniques have been used as well.[10, 11] The rotating disk slurry electrodeposition technique (RoDSE), developed in our laboratory, has been proven to deposit metal nanoparticles on different support materials for bulk production of catalyst powder.[12-18] This technique works by maintaining a circular flux of solution by rotation of the working electrode, constantly replenishing the concentration of the support material and metal ion in the diffusion layer (Figure 1). This allows the electrodeposition of the metal to take place in the conductive support instead of the rotating disk electrode (RDE). To the best of our knowledge, the RoDSE is the only electrochemical synthesis technique where you are able to produce a hybrid material in powder form. Furthermore, no dangerous chemicals, nor strenuous process, are required to complete this electrochemical synthesis. Thus, making RoDSE a valuable technique to produce catalysts for diverse applications. Although the RoDSE method has been successfully used in the past, a fundamental approach is required to further understand and optimize the technique.

In this work, Pd nanoparticles were successfully electrodeposited on Vulcan XC – 72R nanoflakes via the RoDSE technique, at different applied potentials, and tested for the ethanol oxidation reaction in alkaline media. Special care was taken into observing the relationship between the applied electrodeposition potential with morphology, metal loading, size, and catalytic activity.

Experimental methodology

Catalyst preparation

Pd was electrodeposited on Vulcan XC – 72R nanoflake carbon support via the RoDSE technique adapting the same conditions previously reported by Santiago et al.[12, 13] The optimization of RoDSE for the Pd electrodeposition was done by modifying the conditions and optimizing parameters such as the applied potential. Briefly, a slurry suspension was made in a beaker containing 50 mg of Vulcan XC – 72R (from CABOT) and 20 mL of 0.1 M H_2SO_4 (Optima, Aldrich). The suspension was placed under sonication for 8 h to disperse the carbon nanoflake support in order to create a highly dispersed slurry. The resulting suspension was placed in the center of a three–electrode cell assembly for the Pd electrodeposition as seen in Figure 2, i.e. three compartments, each separated by fritted glass. Afterwards, 2.00 mL of a 5.0 mM $PdCl_2$ solution was added to the slurry, in the center glass container. The electrochemical cell was sealed and purged with ultrapure nitrogen for 15 min while the RDE (PINE Instruments Co.) rotated at 1200 rpm in the slurry. The rotating disk working electrode was a glassy carbon electrode (GCE) with a geometric area of 0.20 cm^2. The GCE was previously polished with 1.0, 0.3, and 0.05 μm Al_2O_3 paste (Buehler® Micropolish®) until reaching mirror like state. The residual polishing material was removed from the surface of the GCE by sonication in deionized water bath for 5 min. A high surface area Pt wire and RHE were used as a counter and reference electrodes, respectively.

The Pd electrodeposition was done by applying a constant reductive potential for 2 h in each 2.00 mL additions of 5.0 mM $PdCl_2$ precursor in 0.1M H_2SO_4 solution. This process was repeated 3 additional times. Finally, after the RoDSE process, the slurry was filtered with a 0.22 μm Nylon filter and washed with abundant deionized water. The resulting catalyst material was dried in a 60 °C oven for 24 h and ground to obtain a fine powder.

Electrochemical measurements

Ink paste, for each Pd based catalyst, was prepared by mixing 3 mg of catalyst powder with 150 μL of deionized water, 150 μL of isopropanol (Sigma Aldrich), 300 μL of ethanol (99.5% Sigma Aldrich) and 5 μL of Nafion solution (5 % solution in alcohol, Sigma Aldrich). The mixture was sonicated for 1 h to form the ink paste. Glassy carbon electrodes , (3 mm diameter, from BASi) were polished three times with 1.0, 0.3 and 0.05 μm alumina powder, rinsed and sonicated for 10 minutes in deionized water to remove alumina residue. Afterwards, the GCE were subjected to 5 cycles of a cyclic voltammetry in 0.1 M KOH solution using a potential window of -0.1 to 1.1 V vs. Ag / AgCl, at a potential scan rate of 100 mV/s, to ensure that the resistance and capacitance were in optimal working conditions. Finally, 5 μL of the prepared catalyst ink paste was dropped on the clean GCE surface and was allowed to dry at 60 ºC for 120 s to obtain the modified GCE.

Electrochemical characterization for each Pd / Vulcan catalyst was done under ambient conditions using cyclic voltammetry (CV) in alkaline media. All measurements were done using a PARSTAT 2273 potentiostat. In all experiments, a three electrodes cell was employed

consisting of a Pt wire, reversible hydrogen electrode (RHE) and modified GCE as the auxiliary, reference and working electrodes, respectively.

For all Pd – based catalysts, the electrochemical active surface area (EASA) was calculated to evaluate the current density and thus the catalytic activity of each modified electrode. A charge value of 420 μC cm^{-2} is attributed for the reduction of the PdO monolayer during the cathodic sweep[19], as seen in equation 1.[20] All current densities reported in this work correspond to the EASA of Pd for each catalyst using this method of surface area calculation.

$$Pd - O + H_2O + 2\,e^- \leftrightarrow Pd + 2\,OH^- \quad \text{(Eq. 1)}$$

XRD measurements

The RoDSE synthesized Pd catalysts X – ray diffraction (XRD) patterns were obtained using a Rigaku SmartLab X – ray diffractometer working with a Cu K_α radiation (λ = 1.54 Å) source. The 2Θ range was scanned between 10 - 80° at a rate of 0.02° s^{-1}.

TEM measurements

Transmission electron microscopy images were taken using the JEOL 1400 LaB_6 Soft Bio TEM. A suspension was done by dispersing 5 mg of the catalyst powder in 7.00 mL of pure ethanol by ultra–sonication. A drop of the catalyst suspension was added to a 200 mesh Lacey Carbon copper grid. Particle size histogram was determined using Gatan Digital Micrograph software utilizing different regions of the carbon copper grid to obtain a representative view of each catalysts average particle size

Induced Coupled Plasma – Optical Emmission Spectrometry (ICP – OES)

Palladium metal catalyst loading were measured using an Optima 8000 Perkin Elmer ICP–OES. Briefly, 10 mg of each Pd / Vulcan catalyst was digested with 10 mL of aqua – regia solution and heated to simmering until 1 mL of solution remained. The solutions were passed through a Whatman glass microfiber filter (GF / F grade) and reconstituted with deionized water in a quantitative volumetric flask. Quantification was done in triplicates with an external calibration curve.

TGA measurements

Thermal gravimetric analysis was done using the PerkinElmer STA 6000 thermal analyzer in air with a temperature ramp of 100 °C min^{-1} and maintained at 900 °C for 10 min.

XPS measurements

X–ray photoelectron spectroscopy (XPS) spectra were obtained using a PHI 5600ci spectrometer equipped with an aluminum polychromatic source (350 W) at a 45° angle and a hemispherical electron energy analyzer. The pass energy was 58.70eV. A small sample of the catalytic powder was pressed onto copper tapes.

Results and Discussion

Pd electrodeposition

Cyclic voltammetry was performed utilizing a clean glassy carbon electrode in a 5 mM $PdCl_2$ precursor solution (Figure 3). This was done to identify the different thermodynamic and kinetic regimes of the Pd reduction reaction and apply this knowledge to the RoDSE technique. A starting potential of 1.6 V was chosen to make sure that the Pd^{2+} ions were in solution. In the first scan, a cathodic peak, near 0.53 V, corresponds to the deposition of Pd onto the glassy carbon electrode. Afterwards, for each cycle, a characteristic Pd voltammogram is appreciated with higher currents for each cycle due to the deposition of more Pd as the cycles advance. Cathodic and anodic peaks between 0.05 and 0.2 V correspond to the H_2 ad/absorption and desorption, respectively. Three different applied potentials (0.0, 0.4 and 0.7 V vs. RHE) were chosen for the electrodeposition of Pd on the carbon support by the RoDSE methodology. Each applied potential may corresponds to a different thermodynamic or kinetic region for the reduction of Pd. At more negative potentials a mass transport controlled reduction (fast) occurs whereas the applied potential becomes more positive, a kinetically controlled deposition (slower) occurs. However, the electrodeposition in slurry may differ from the electrodeposition in solution, particularly the presence of flakes can result in the depolarization of Pd deposition.

Figure 4 demonstrate the successful deposition of Pd on Vulcan XC–72R nanoflakes by the RoDSE technique at all applied potentials by the cathodic current obtained for each added aliquot of the precursor solution. However, it is noticeable that the average deposition current decreases as the potential becomes more positive. At applied deposition potentials of 0.0, 0.4, and 0.7V vs RHE the average maximum deposition current was -1.3, -0.9, and -0.3 mA, respectively. This occurs because, as the applied potential is more positive, a slower, milder, electrodeposition of Pd occurs on the surface of the carbon support.

XRD measurements

XRD analysis was done for each of the synthesized Pd/Vulcan nanoflakes catalyst to verify the palladium patterns. XRD patterns of all samples (Figure 5) show three peaks at 2Θ = 40.0°, 46.5°and 68.1° corresponding to the (111), (200) and (220) planes of the Pd face center cubic structure, respectively.[21] A broad peak appears at 25.0° corresponding to the (200) plane of Vulcan XC–72R nanoflakes.

TEM measurements

After confirming the successful deposition and understanding the crystalline structure of the deposited palladium nanoparticles on the carbon support, TEM was used to determine particle size and dispersion for each Pd electrodeposition (Figure 6). There is a clear indication that, at negative potentials (0.0 V vs. RHE), agglomeration occurs. This results in Pd islands with occasional, relatively small, Pd nanoparticles. However, as the electrodeposition potential becomes more positive (0.4 V vs. RHE), it becomes apparent that the Pd islands are less frequent and smaller. At this same potential, smaller Pd nanoparticles can be found frequently and

homogenously dispersed on the carbon support. Finally, at the other boundary of the applied potential (0.7 V vs. RHE), we can see that there is no apparent Pd island formation and there are small and well dispersed palladium nanoparticles. These results concur with the results obtained in the electrodeposition process. At stronger electrodeposition potential (0.0 V vs. RHE) a higher deposition current was obtained indicating that palladium was being deposited in a more aggressive way thus making agglomeration favorable. However, as the electrodeposition potential is weaker, less electrodeposition current is obtained stipulating a milder deposition of palladium on the carbon support, consequently, less agglomeration occurs. However, this also leads us to suspect less palladium deposited by mass as the applied potential is milder.

Even though a small amount of subjects were obtained, a particle size histogram was done for each synthesized Pd / Vulcan catalyst (Figure 7). It was found that the synthesis using 0.7 V vs. RHE, contained smaller and well dispersed palladium nanoparticles, with an average of 6 nm, deposited on Vulcan XC–72R nanoflakes than the catalyst synthesized at 0.0 and 0.4 V vs. RHE. It is notable to mention that, as the RoDSE electrodeposition potential is increased, a smaller amount of palladium nanoparticles are observed deposited on the carbon support. This suggests that a smaller amount of palladium by mass is deposited on the Vulcan XC–72R nanoflake support.

Inductively Couple Plasma – Optical Emission Spectroscopy (ICP – OES)

In order to corroborate the hypothesis that at higher potentials, lower palladium was deposited, each Pd / Vulcan nanoflake catalyst was analyzed by ICP – OES. The analytical percentage of the total Pd loading in each catalyst sample are shown in Table 1. It is clear that the Pd / Vulcan nanoflake catalyst synthesized at 0.0 V contains the most Pd by mass followed by 0.4 and 0.7 V, respectively. These results indicate that as the applied potential is more positive, less Pd by mass is deposited on the carbon support. These results agree with the TEM images, as it was more challenging to find Pd metal deposited on the carbon support for more positive applied potentials. These results validate our initial hypothesis that at milder potential less amount of palladium, by mass, is deposited on the carbon support.

Thermal Gravimetric Analysis (TGA)

To confirm the Pd loading in Vulcan XC–72R nanoflakes and understand the thermal stability of each synthesized catalyst, TGA was done in air. Figure 8 (top) demonstrates the thermal decomposition of all the synthesized Pd / Vulcan nanoflake catalysts. It is clear that at low temperatures all catalysts have the same thermal behavior, however as the temperature increases the weight percentage, of the catalyst synthesized at 0.7 V vs RHE, decays more rapidly than its two counterparts, suggesting that the catalyst synthesized at 0.7 V is less thermally stable than the catalysts synthesized at 0.0 V and 0.4 V vs RHE. After reaching 900 °C (bottom), the Pd loading were 6.87%, 6.54% and 4.43% for the catalyst synthesized at 0.0, 0.4 and 0.7 V, respectively. These results follow the same trend as the ICP – OES results although with higher mass loading, found by TGA, may de due to the formation of PdO layer at high temperature.[22] The faster decrease in mass for the Pd / Vulcan catalyst synthesized at 0.7 V vs. RHE may be due to the considerable decrease of deposited palladium by mass and larger amounts of carbon

functionalities, as observed by XPS. As less palladium is deposited, more of the Vulcan XC – 72R nanoflake surfaces are in contact with supporting electrolyte solution. As the applied potential is slightly oxidative for the carbon support, more oxygen defects are formed on the surface of the carbon support. This would allow for easier combustion and, consequently, a faster decrease in mass for the catalyst synthesized at 0.7 V vs. RHE. However, 0.4 V vs. RHE is not sufficiently positive to oxidize Vulcan XC – 72R as much as 0.7 V vs. RHE, whereas less oxygen defect are formed and higher thermal stability is observed.

X – Ray Photoelectron Spectroscopy (XPS)

To understand the chemical effect of the applied potential on the Pd RoDSE deposition on Vulcan XC – 72R nanoflakes, XPS was done for each catalyst. XPS results for Pd 3d, O 1s and C 1s binding energy regions were analyzed using curve – fitting program (Multipack) for peak deconvolution. The peak assignments for the C 1s components are shown in Table 2.[23] The O 1s binding energy peak assignments were ~530.3 eV, ~552 eV and ~533 eV, attributed to PdO[24], C-O[25] and C=O[25], respectively.

Figure 9 shows the C 1s and O 1s binding energy spectra regions obtained by XPS for the synthesized catalysts samples, as well as the peak deconvolution for each sample. The Pd 3p binding energy peaks usually overlaps with the O 1s peak.[24] However, all catalyst sample showed a minimal Pd signal, within the noise level. The highest was for the catalyst prepared with a 0V applied potential, which showed 0.5% in Pd when compared with O and C. Therefore, the 3p binding energy peak should be in the noise level, as well. The abundance of carbon Vulcan nanoflakes may block the 3p and 3d Pd electrons. Since the presence of Pd was observed by cyclic voltammetry, XRD and TGA, the O 1s binding energy peak was fitted assuming contribution from the oxygen of PdO functionalities. The C 1s peak contains various features that could not be fully resolved. Instead of fitting all 6 components, the peak deconvolution was carried out as described in Table 3 and the contribution for each component of the C 1s and O 1s are described in Table 4.

The O 1s XPS binding energy peak showed that the applied electrodeposition potential greatly affected the amount of oxygen containing species on the synthesized catalysts. It can be observed from the spectra, that for the 0.0 V vs. RHE electrodeposition sample there was very little oxygen contribution when compared with the other two catalysts samples. The majority of the oxygen XPS binding energy signal, for the 0.0 V vs. RHE electrodeposition catalyst sample, came from PdO. In general, the amount of oxygen functionalities increased concomitant with more positive electrodeposition potential. Congruently, The relative amount of PdO decreased with a more positive electrodeposition potential. It may be concluded that with a more positive applied electrodeposition potential, more oxidized carbon species are available in the Vulcan XC-72R nanoflake matrix.

The carbon 1s binding energy peak component and XPS spectra supported the conclusions obtained from the O 1s binding energy region. Although all the C 1s peak components could not be resolved, the sp^2 and sp^3 components, in addition to the π-π^* transition, gave valuable insight into the carbon matrix. For the 0.0 V electrodepositon sample showed the highest amount of π-π^*

transition and graphitic carbon, indicating that it has the lowest amount of oxygen functionalities in the carbon Vulcan support. For the 0.4V and 0.7V vs. RHE applied potential, the amount of sp^2 carbon decreases, the amount of sp^3 carbon increases and the π-π^* transition disappears compared to the 0.0V vs. RHE sample. This means that at more positive applied electrodeposition potential, more oxygen containing species in the carbon matrix are observed. The higher amount of nucleation sites, due to the oxygen functionalities on the carbon support, may explain the dispersion of the synthesized catalysts and their relative sizes. The TGA results agree with these conclusions suggesting that the catalyst synthesized at 0.7 V vs. RHE has more oxygen containing species making thermal decomposition at lower temperature when compared to catalysts synthesized at 0.0 V and 0.4 V vs. RHE. Therefore, the catalyst synthesized at 0.7 V vs. RHE is less thermally stable.

Electrochemical Measurement

The electrocatalytic activity, towards ethanol oxidation reaction (EOR) in alkaline media, for each Pd / Vulcan catalyst was tested by cyclic voltammetry. Figure 10A shows cyclic voltammograms in 0.1 M KOH of modified glassy carbon electrodes with all the synthesized Pd / Vulcan catalysts. Cathodic peaks observed at 0.65 V vs. RHE are due to the reduction of the PdO monolayer formed in the anodic sweep.[20] However, the foremost difference with each CV consists in the difference of the capacitance double layer current which is directly proportional to the applied potential used to deposit Pd on Vulcan XC – 72R. This effect is due to the lesser amount of Pd, by mass, deposited on the carbon support as the synthesis potential is more positive, as demonstrated by the ICP – OES and TGA results. As less Pd is present in the catalyst, more carbon surface area is in contact with solution so a higher capacitance current is observed. In addition to the amount of Pd, it has been shown that the capacitance current also increases due to surface oxidation defects on the carbon surface.[26, 27] XPS spectra clearly demonstrated the direct correlation between the applied potential and the surface oxidation defects on Vulcan XC–72R. Both factors, the amount of Pd deposited and the oxidation defects on Vulcan XC–72R, caused by the applied potential, contribute to the difference in the capacitance current for each catalyst.

The catalytic activity for each Pd/Vulcan nanoflake catalyst was examined by cyclic voltammetry for EOR in alkaline media (Figure 10B). There are two peaks corresponding to ethanol oxidation. In the anodic sweep, an ethanol oxidation peak appears between 0.81 to 0.84 V vs. RHE, for the three catalysts. These peaks are attributed to the ethanol electrooxidation by adsorbed oxygen containing species of Pd ($Pd–OH_{ads}$) which form in alkaline media.[20] However, beyond 0.84 V vs. RHE the current density decreases as the potential is increased until the current concurs with the base current. This is due to Pd (II) oxide layer formation on the surface of the nanoparticles, which blocks the active Pd species leading to a decrease in the electrocatalytic activity. In the cathodic sweep, lower than 0.65V vs. RHE, the ethanol oxidation reaction reoccurs due to the reduction of the Pd (II) oxide layer recovering the electrocatalytic activity of the catalysts. The onset ethanol oxidation reaction current density potential was more negative for Pd/Vulcan catalyst synthesized at 0.4V vs. RHE. This catalyst had the highest

ethanol oxidation peak current density, as well. In the cathodic sweep, this catalyst maintained an ethanol oxidation current density at more negative potentials than the other two catalysts.

It is notable that, even with less Pd loading, the Pd catalyst synthesized at 0.7 V vs. RHE had a slightly higher current density than the Pd catalyst synthesized at 0.0 V vs. RHE. This is due to the smaller nanoparticles deposited on the carbon support, as seen in the TEM images, due to the milder electrodeposition applied potentials. The cyclic voltammetry results suggest that, for the RoDSE methodology, applying a deposition potential between the mass transport and kinetic region of where Pd deposits on carbon, provides the optimal electrochemical Pd catalyst preparation conditions for EOR.

Conclusions

In this work, the effect of the applied potential used in the Pd electrodepositon on Vulcan XC-72R nanoflakes by RoDSE methodology was studied. It was found that, independently of the applied potential, polycrystalline Pd nanoparticles deposits on the Vulcan nanoflake support. However, results from TEM, ICP–OES and TGA demonstrates that, as the applied potential is more positive, the Pd nanoparticles are of a smaller size but less Pd by mass is deposited on the carbon support. This is due because as the applied potential is more positive, XPS results demonstrate that there are more oxygen species on the carbon support, making home for more nucleation sites for smaller and less agglomerated Pd nanoparticles. However, these oxygen defects on Vulcan XC–72R also lead to faster thermal decomposition as seen in the TGA results.

Even though the deposition of Pd at 0.7 V vs. RHE demonstrated smaller nanoparticles, the synthesis done at 0.4 V vs. RHE demonstrated higher electrocatalytic activity towards ethanol oxidation. This suggests that applying potential between the kinetic and mass transport region, for the deposition of Pd nanoparticles using the RoDSE methodology, provides good balance between the metal electrodeposition yield and the particle size and formation for ethanol electrooxidation reaction in alkaline media. Applying 0.4 V vs. RHE, in the RoDSE electrodeposition process, provided the optimal conditions to produce a Pd nanocatalyst with high electrodeposition yield (83.3%), low agglomeration, thermally stable, and relatively small nanoparticles, which leads to better EOR.

Acknowledgements

This work was financially supported by the NSF-CREST Center for Innovation Research and Education in Environmental Nanotechnology Grant Number HRD-1736093 and NASA-EPSCoR grant number NNX14AN18A. This research used resources of the Center for Functional Nanomaterials (CFN), which is a U.S. DOE Office of Science Facility, at Brookhaven National Laboratory (BNL) under Contract No. DE-SC0012704. CAV thanks Kim Kisslinger (CFN-BNL) for assistance on the TEM images.

References

1. E. Antolini and E. R. Gonzalez, *J. Power Sources,* **195** (11), 3431-3450 (2010).
2. G. Merle, M. Wessling, and K. Nijmeijer, *J. Membr. Sci.,* **377** (1–2), 1-35 (2011).
3. N. A. Tapan, M. E. Günay, and R. Yildirim, *Chem. Eng. Res. Des.,* **105** 162-170 (2016).
4. S. P. S. Badwal, S. Giddey, A. Kulkarni, J. Goel, and S. Basu, *Appl. Energy,* **145** (0), 80-103 (2015).
5. H. Hou, S. Wang, W. Jin, Q. Jiang, L. Sun, L. Jiang, and G. Sun, *Int. J. Hydrogen Energy,* **36** (8), 5104-5109 (2011).
6. D. Jacobsen and K. E. McMartin, *J. Toxicol. Clin. Toxicol.,* **35** (2), 127-143 (1997).
7. E. Antolini, J. R. C. Salgado, R. M. da Silva, and E. R. Gonzalez, *Mater. Chem. Phys.,* **101** (2–3), 395-403 (2007).
8. D. Shah and H. Kaur, *J. Mol. Catal. A: Chem.,* **424** 171-180 (2016).
9. A. V. Kobets and T. N. Vorobyova, *Thin Solid Films,* **616** 793-799 (2016).
10. S. Choi, H. Jeong, K.-h. Choi, J. Y. Song, and J. Kim, *ACS Appl. Mater. Interfaces,* **6** (4), 3002-3007 (2014).
11. H. Jeong and J. Kim, *ACS Appl. Mater. Interfaces,* **7** (13), 7129-7135 (2015).
12. D. Santiago, G. G. Rodríguez-Calero, H. Rivera, D. A. Tryk, M. A. Scibioh, and C. R. Cabrera, *J. Electrochem. Soc.,* **157** (12), F189-F195 (2010).
13. D. Santiago, G. G. Rodríguez-Calero, A. Palkar, D. Barraza-Jimenez, D. H. Galvan, G. Casillas, A. Mayoral, M. Jose-Yacamán, L. Echegoyen, and C. R. Cabrera, *Langmuir,* **28** (49), 17202-17210 (2012).
14. E. Contes-de Jesus, D. Santiago, G. Casillas, A. Mayoral, C. Magen, M. José-Yacaman, J. Li, and C. R. Cabrera, *J. Electrochem. Soc.,* **160** (2), H98-H104 (2012).
15. L. Cunci, C. A. Velez, I. Perez, A. Suleiman, E. Larios, M. José-Yacamán, J. J. Watkins, and C. R. Cabrera, *ACS Appl. Mater. Interfaces,* **6** (3), 2137-2145 (2014).
16. A. Suleiman, C. L. Menendez, R. Polanco, E. R. Fachini, Y. Hernandez-Lebron, M. J. F. Guinel, R. Roque-Malherbe, and C. R. Cabrera, *RSC Adv.,* **5** (10), 7637-7646 (2015).
17. L. E. Betancourt, R. Guzmán-Blas, S. Luo, D. J. Stacchiola, S. D. Senanayake, M. Guinel, and C. R. Cabrera, *Electrocatalysis,* 1-8 (2016).
18. J. A. Banuelos, O. Garcia-Rodriguez, F. J. Rodriguez-Valadez, and L. A. Godinez, *J. Electrochem. Soc.,* **162** (9), E154-E159 (2015).
19. L.-l. Fang, Q. Tao, M.-f. Li, L.-w. Liao, D. Chen, and Y.-x. Chen, *Chin. J. Chem. Phys.,* **23** (5), 543-548 (2010).
20. Z. X. Liang, T. S. Zhao, J. B. Xu, and L. D. Zhu, *Electrochim. Acta,* **54** (8), 2203-2208 (2009).
21. F. Wang, L. Yang, Q. Tang, Y. Guo, and G. Hao, *Catal. Sci. Technol.,* **3** (5), 1246-1252 (2013).
22. S. J. Cho and S. K. Kang, *J. Phys. Chem. B,* **104** (34), 8124-8128 (2000).
23. R. I. R. Blyth, H. Buqa, F. P. Netzer, M. G. Ramsey, J. O. Besenhard, P. Golob, and M. Winter, *Appl. Surf. Sci.,* **167** (1–2), 99-106 (2000).
24. M. Peuckert, *J. Phys. Chem. B,* **89** (12), 2481-2486 (1985).
25. S. M. Senthil Kumar, J. Soler Herrero, S. Irusta, and K. Scott, *J. Electroanal. Chem.,* **647** (2), 211-221 (2010).
26. K. H. Kangasniemi, D. A. Condit, and T. D. Jarvi, *J. Electrochem. Soc.,* **151** (4), E125-E132 (2004).
27. C. A. Frysz and D. D. L. Chung, *Carbon,* **35** (8), 1111-1127 (1997).

Figures

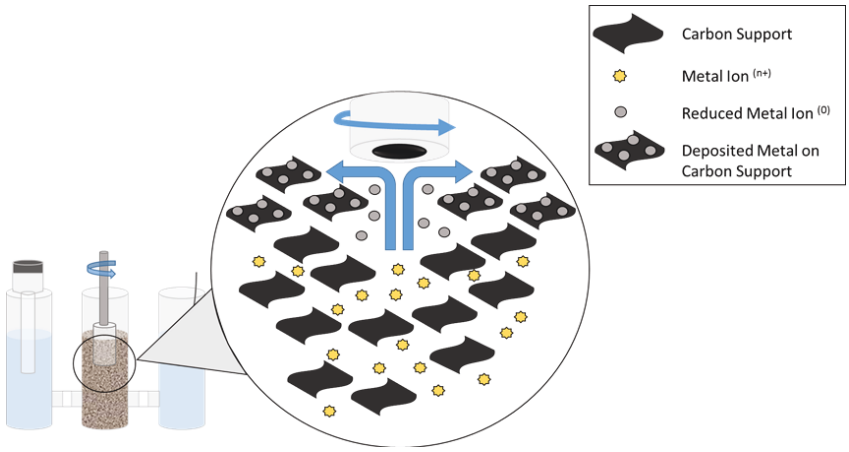

Figure 1. General scheme of the electrochemical deposition of metal nanoparticles onto a carbon support via the RoDSE methodology.

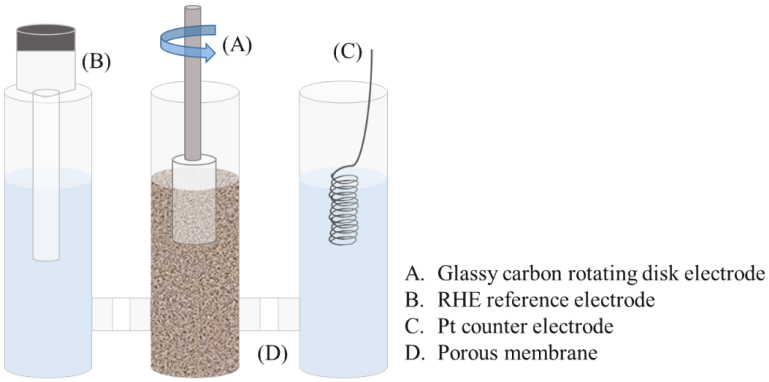

Figure 2. RoDSE electrochemical cell setup showing the placement of the working electrode, reference electrode, counter electrode and the porous membrane separating each compartment.

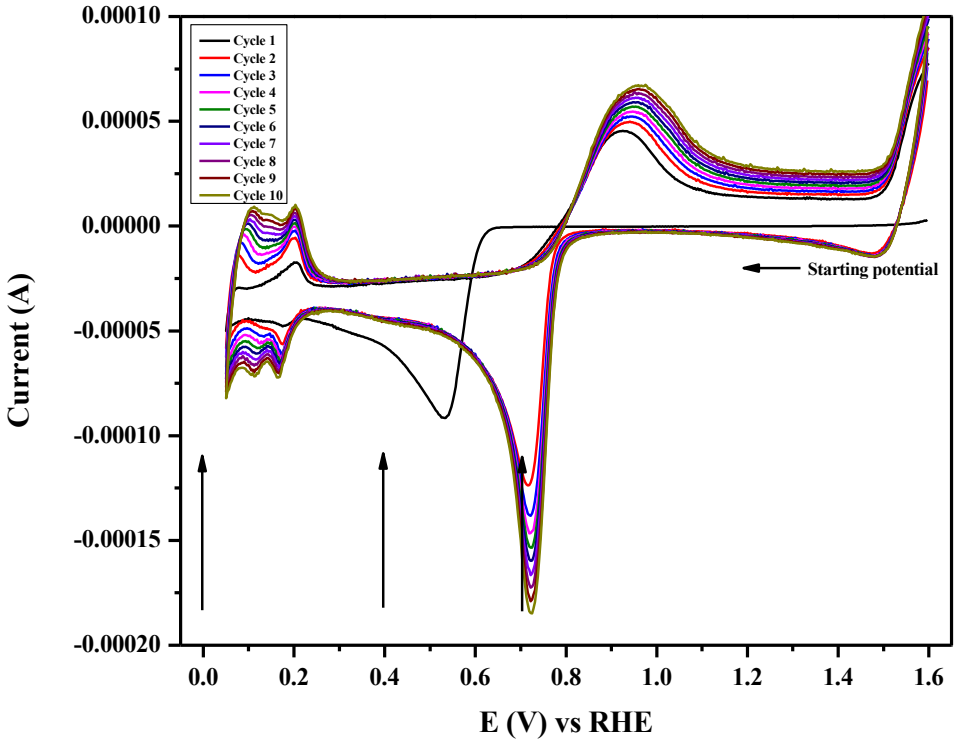

Figure 3. Cyclic voltammograms of a clean glassy carbon electrode in a 5 mM $PdCl_2$ / 0.1 M H_2SO_4 solution at 25 mV / s. Arrows indicate the three different applied potential used for the Pd electrodeposition using the RoDSE method.

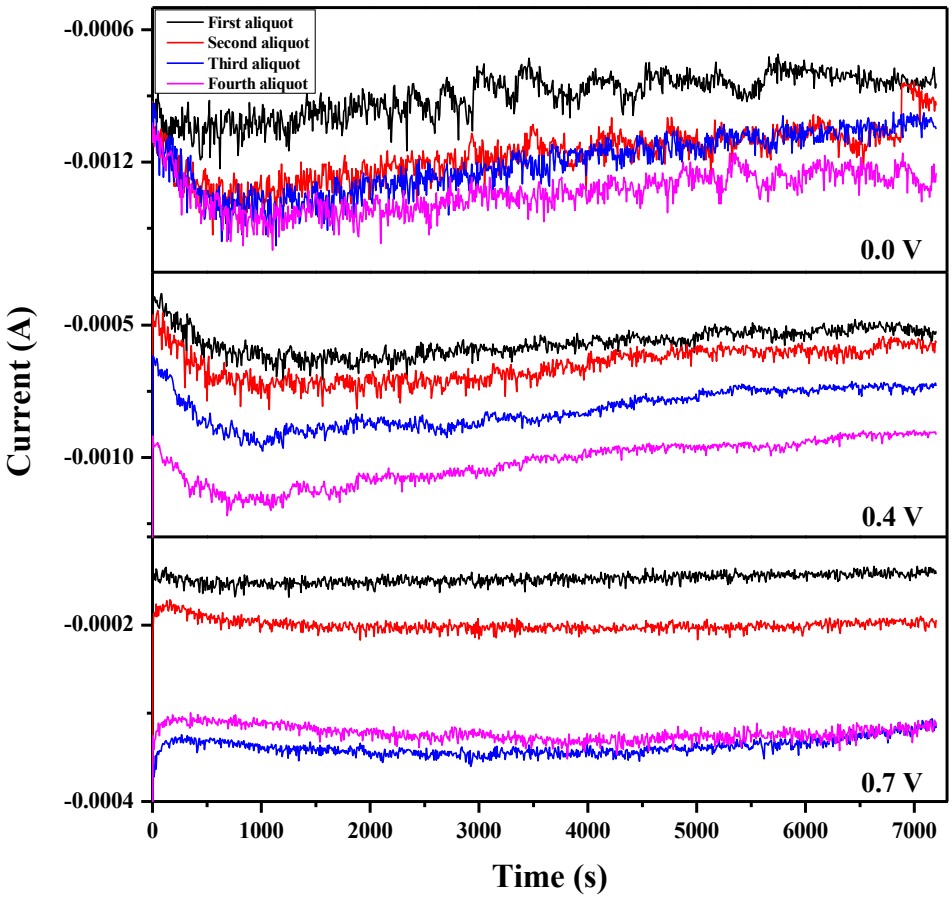

Figure 4. Current vs. time graphs for the Pd electrodeposition in 20 mL of a Vulcan XC – 72R nanoflake slurry in 0.1 M H_2SO_4 at different applied potentials; 0.0, 0.4 and 0.7V vs. RHE. For each applied potential, four consecutive electrodepositions were done. In each electrodeposition, a 2mL aliquot 5 mM $PdCl_2$ / 0.1 M H_2SO_4 solution was added to the slurry.

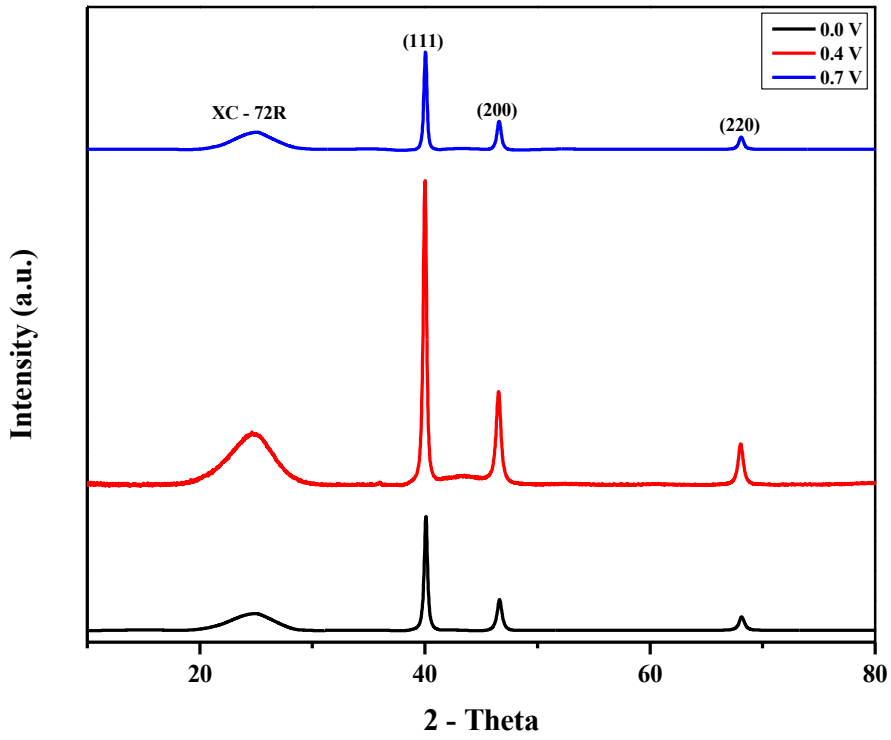

Figure 5. XRD pattern for the Pd / Vulcan XC – 72R nanoflake catalyst synthesized by RoDSE at 0.0 V (black), 0.4 V (red) and 0.7 V (blue) vs. RHE applied potentials.

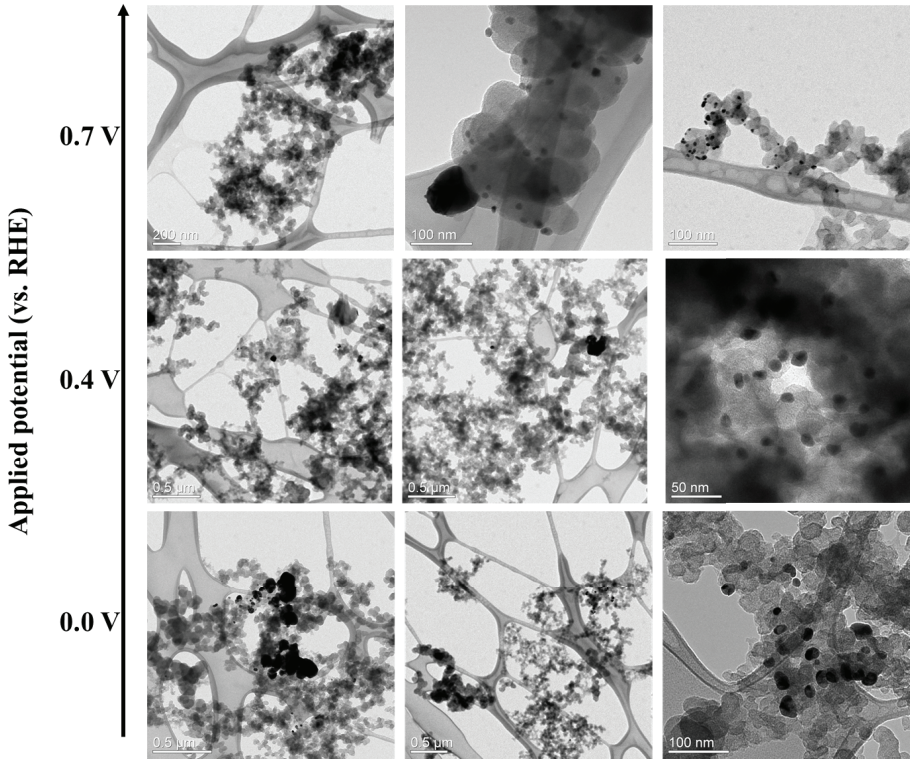

Figure 6. Transmission electron microscopy images, at different magnifications, of the Pd / Vulcan XC – 72R nanoflake catalysts synthesized by RoDSE at 0.0 V (bottom, scale bar: 0.5µm; 0.5µm; 100nm from left to right), 0.4 V (middle, scale bar: 0.5µm; 0.5µm; 50nm from left to right) and 0.7 V (top, scale bar: 200nm; 100nm; 100nm from left to right) vs. RHE applied potentials.

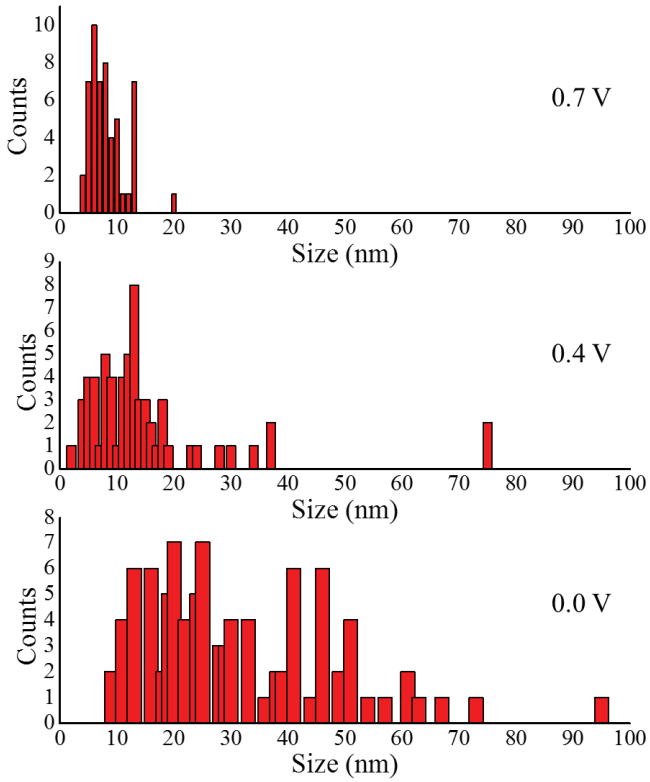

Figure 7. Particle size histogram from TEM images of each Pd / Vulcan XC 72R nanoflakes catalyst synthesized at 0.0 V (bottom), 0.4 V (middle) and 0.7 V (top) vs. RHE with a total particle count of 92, 60 and 53, respectively.

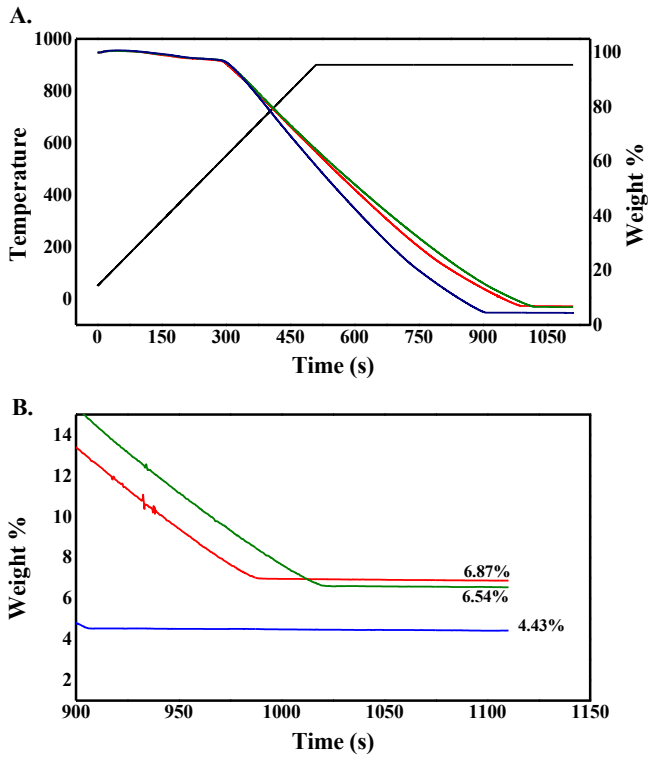

Figure 8. Thermal gravimetric analysis, in air, with a temperature ramp of 100 °C min^{-1} and maintained at 900 °C for 10 min, for the Pd / Vulcan XC – 72R nanoflake catalyst synthesized by RoDSE at 0.0 V (red), 0.4 V (green) and 0.7 V (blue) vs. RHE applied potentials. (B) Weight percentage obtained for each synthesized Pd / Vulcan XC – 72R nanoflake catalyst after the conclusion of the analysis.

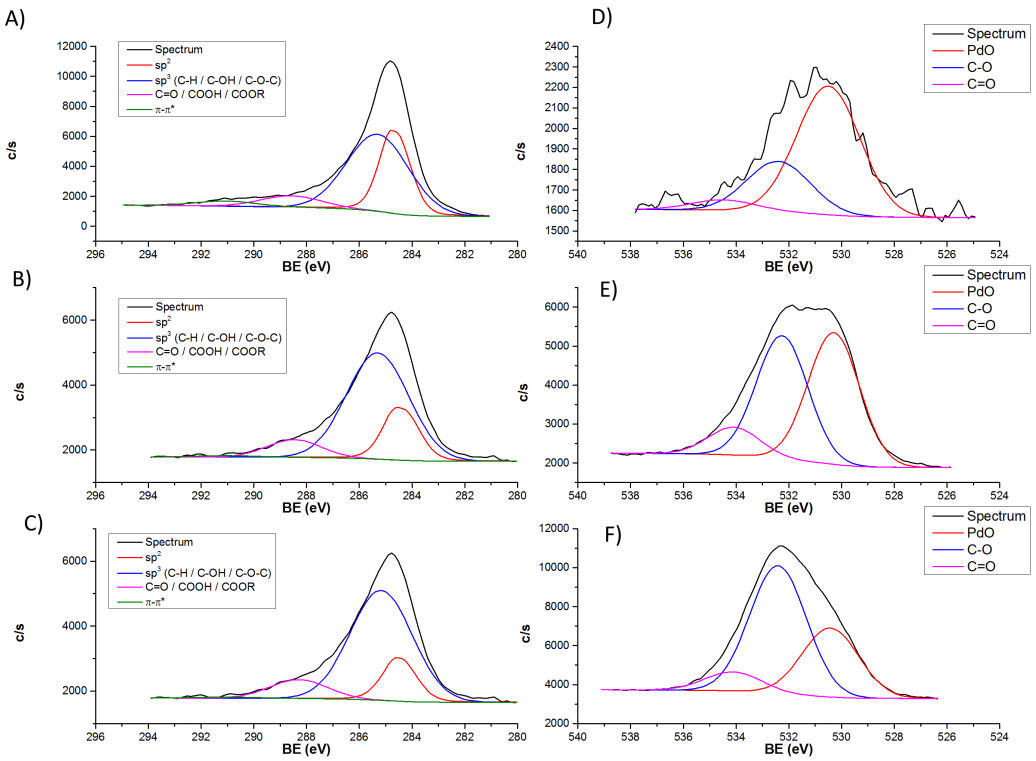

Figure 9. (A – C) C 1s and (D – F) O 1s XPS spectra of the Pd / Vulcan XC – 72R nanoflake catalyst synthesized by RoDSE at (A and D) 0.0 V, (B and E) 0.4 V and (C and F) 0.7 V vs. RHE applied potentials.

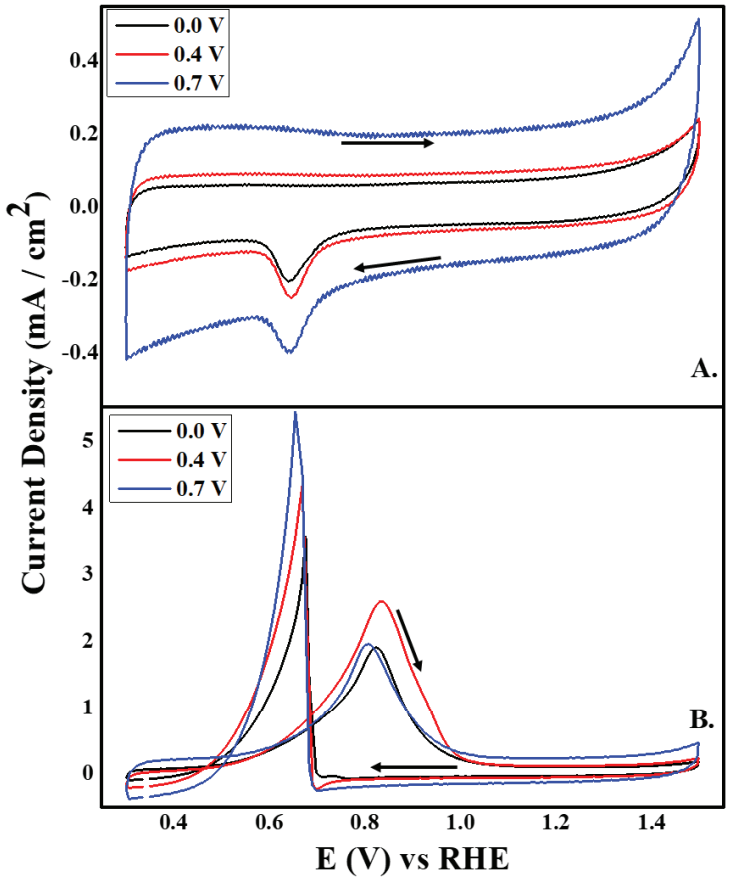

Figure 10. Cyclic voltammograms in (A) 0.1 M KOH and (B) 0.5 M EtOH / 0.1 M KOH for the Pd/Vulcan XC–72R nanoflake catalyst synthesized by RoDSE at 0.0 V, 0.4 V and 0.7 V vs. RHE applied potentials. The scan rate was 25 mV/s. Arrows indicate the potential sweep direction.

Tables

Table 1. Metal % m/m for each Pd / Vulcan catalyst synthesized at different applied potentials.

Applied potential (V vs RHE)	Metal percentage (% m/m)
0.0	6.43 %
0.4	5.04 %
0.7	3.81 %

Table 2. X-ray photoelectron spectroscopy C 1s binding energy peak assignments

Carbon 1s Components	**Binding Energy (eV)**
Graphite (sp^2)	284.4
C-H (sp^3)	285.0
C-OH / C-O-C (sp^3)	286.1 – 286.3
C=O	287.6 – 287.7
COOH / COOR	288.6 – 289.1
π-π*	290.5 – 290.8

Table 3: Simplification of C 1s components for X-ray photoelectron spectroscopy binding energy peak deconvolution.

Carbon 1s Components	**Binding Energy (eV)**
sp^2	~284.7
sp^3/ C-OH/ C-O-C	~285.4
C=O / COOH / COOR	~288.7
π-π*	~291.0

Table 4: Contribution for the C 1s and O 1s binding energy components of the X-ray photoelectron spectroscopy measurements shown in Figure 8 for each Pd/Vulcan XC–72R nanoflake catalyst synthesized by RoDSE at 0.0 V, 0.4 V and 0.7 V vs. RHE applied potentials.

	Carbon 1s Component % Contribution				Oxygen 1s Component % Contribution		
Sample	sp^2	sp^3/ C-OH/ C-O-C	C=O / COOH / COOR	π-π^*	PdO	C-O	C=O
0.0 V	45.3%	43.4%	8.3%	3.0%	67.9%	26.6%	5.5%
0.4 V	23.5%	66.6%	9.2%	0.7%	46.6%	43.6%	9.8%
0.7 V	17.7%	77.6%	4.7%	0.0%	32.0%	59.2%	8.8%